dispersion of the Karin family requires that its parent body was pre-fragmented or reaccumulated. This supports the overall picture that all large members of asteroid families are reaccumulated bodies, given that the Karin cluster is at least a second-generation family in the lineage of the older Koronis parent body.

Our simulations can also be used to determine the impact energy needed to produce a given degree of disruption as a function of the internal structure of the parent body. From Table 1, we see that disrupting a pre-shattered target requires less energy per unit mass than for a monolithic body. This, at first glance a surprising result, is related to the fact that the fractures as modelled here (no porosity and no material discontinuities except damage) do not affect shock waves but only tensile waves. Hence, fragments can be set in motion immediately upon being hit by the shock wave without having to wait for fracture to occur in a following tensile wave. Thus, transfer of momentum is more efficient and disruption facilitated. Note that the presence of large voids such as those in rubble piles affect the propagation of the shock wave, thus reversing this trend. A more detailed study of these properties will be presented in another paper. Nevertheless, it is already clear that the internal structure of an asteroid plays an important role in the determination of its response to impacts (see also ref. 18). This is not only relevant for estimating the collisional lifetime of a body in the asteroid belt, but also for developing strategies to deflect a potential Earth impactor.

A last important implication of our simulations concerns the properties of family members with sizes smaller than can currently be observed. The break-up of a pre-shattered Karin parent body produces several thousand fragments with sizes ranging from a few kilometres down to our resolution limit of 0.2 km (Fig. 1). Their ejection speeds can allow some of them to be injected into efficient transport mechanisms leading to Earth-crossing orbits. Therefore, we conclude that the Karin break-up event may well have produced some near-Earth asteroids and even some meteorities. According to our simulations, the potential near-Earth asteroids with size at least above 0.2 km result from the gravitational reaccumulation of smaller fragments, and are therefore all aggregates. □

Received 4 October; accepted 5 December 2002; doi:10.1038/nature01364.

1. Milani, A. & Knežević, Z. Asteroid proper elements and the dynamical structure of the asteroid main belt. *Icarus* **107,** 219–254 (1994).
2. Zappalà, V., Bendjoya, P., Cellino, A., Farinella, P. & Froeschlé, C. Asteroid families: Search of a 12,487-asteroid sample using two different clustering techniques. *Icarus* **116,** 291–314 (1995).
3. Farinella, P., Davis, D. R. & Marzari, F. in *Completing the Inventory of the Solar System* (eds Rettig, T. W. & Hahn, J. M.) 45–55 (ASP Conference Series 107, Astronomical Society of the Pacific, San Francisco, 1996).
4. Marzari, F., Farinella, P. & Davis, D. R. Origin, aging, and death of asteroid families. *Icarus* **142,** 63–77 (1999).
5. Bottke, W. F., Vokrouhlický, D., Brož, M., Nesvorný, D. & Morbidelli, A. Dynamical spreading of asteroid families via the Yarkovsky effect. *Science* **294,** 1693–1696 (2001).
6. Nesvorný, D., Bottke, W. F., Dones, L. & Levison, H. F. The recent breakup of an asteroid in the main-belt region. *Nature* **417,** 720–722 (2002).
7. Michel, P., Benz, W., Tanga, P. & Richardson, D. C. Collisions and gravitational reaccumulation: Forming asteroid families and satellites. *Science* **294,** 1696–1700 (2001).
8. Michel, P., Benz, W., Tanga, P. & Richardson, D. C. Formation of asteroid families by catastrophic disruption: Simulations with fragmentation and gravitational reaccumulation. *Icarus* **160,** 10–23 (2002).
9. Melosh, J. G. & Ryan, E. V. Asteroids: shattered but not dispersed. *Icarus* **129,** 562–564 (1997).
10. Tillotson, J. H. *Metallic Equations of State for Hypervelocity Impact* (General Atomic Report GA-3216, San Diego, 1962).
11. Thompson, S. L. & Lauson, H. F. Improvement in the chart D radiation hydrodynamic code III: revised analytic equation of state. (Report SC-RR-71 0714, Sandia National Laboratory, Albuquerque, 1972).
12. Belton, B. *et al.* The bulk density of asteroid 243 Ida from Dactyl's orbit. *Nature* **374,** 785–788 (1995).
13. Yeomans, D. K. *et al.* Radio science results during the NEAR-Shoemaker spacecraft rendezvous with Eros. *Science* **289,** 2085–2088 (2000).
14. Flynn, G. J., Moore, L. B. & Klöck, W. Density and porosity of stone meteorites: implications for the density, porosity, cratering, and collisional disruption of asteroids. *Icarus* **142,** 97–105 (1999).
15. Bottke, W. F., Nolan, M. C., Greenberg, R. & Kolvoord, R. A. Velocity distributions among colliding asteroids. *Icarus* **107,** 255–268 (1994).
16. Benz, W. & Asphaug, E. Catastrophic disruptions revisited. *Icarus* **142,** 5–20 (1999).
17. Richardson, D. C., Quinn, T., Stadel, J. & Lake, G. Direct large-scale *N*-body simulations of planetesimal dynamics. *Icarus* **143,** 45–59 (2000).
18. Asphaug, E. *et al.* Disruption of kilometre-sized asteroids by energetic collisions. *Nature* **393,** 437–440 (1998).

Acknowledgements P.M. acknowledges financial support from the Action Thématique Innovante 2001 of the French INSU, the programme 'Bonus-Qualité-Recherches 2001' and the Cassini laboratory of the Côte d'Azur Observatory (OCA). W.B. and D.C.R. acknowledge support respectively from the Swiss National Science Foundation and NASA through the Office of Space Science. Simulations were carried out on 4-processor Compaq DEC Alpha workstations thanks to the SIVAM project and the ILGA team of the OCA and on a Beowulf installed by the society Alineos.

Competing interests statement The authors declare that they have no competing financial interests.

Correspondence and requests for materials should be addressed to P.M. (e-mail: michel@obs-nice.fr).

Attosecond control of electronic processes by intense light fields

A. Baltuška*, Th. Udem†, M. Uiberacker*, M. Hentschel*, E. Goulielmakis*, Ch. Gohle†, R. Holzwarth†, V. S. Yakovlev*, A. Scrinzi*, T. W. Hänsch† & F. Krausz*

** Institut für Photonik, Technische Universität Wien, Gusshausstrasse. 27, A-1040 Wien, Austria*
† Max-Planck-Institut für Quantenoptik, Hans-Kopfermann-Strasse 1, D-85748 Garching, Germany

The amplitude and frequency of laser light can be routinely measured and controlled on a femtosecond (10^{-15} s) timescale[1]. However, in pulses comprising just a few wave cycles, the amplitude envelope and carrier frequency are not sufficient to characterize and control laser radiation, because evolution of the light field is also influenced by a shift of the carrier wave with respect to the pulse peak[2]. This so-called carrier-envelope phase has been predicted[3–9] and observed[10] to affect strong-field phenomena, but random shot-to-shot shifts have prevented the reproducible guiding of atomic processes using the electric field of light. Here we report the generation of intense, few-cycle laser pulses with a stable carrier envelope phase that permit the triggering and steering of microscopic motion with an ultimate precision limited only by quantum mechanical uncertainty. Using these reproducible light waveforms, we create light-induced atomic currents in ionized matter; the motion of the electronic wave packets can be controlled on timescales shorter than 250 attoseconds (250×10^{-18} s). This enables us to control the attosecond temporal structure of coherent soft X-ray emission produced by the atomic currents—these X-ray photons provide a sensitive and intuitive tool for determining the carrier-envelope phase.

Matter exposed to intense laser light undergoes ionization, which gives rise to a broad range of phenomena in atoms, molecules and plasmas. An electronic wave packet is set free around each oscillation peak of a laser electric field that is strong enough to overcome the effective binding potential (Fig. 1a). The ensuing motion of the wave packets released by optical-field ionization depends on the subsequent evolution of the driving laser field[11,12]. A laser pulse consisting of many wave cycles launches a number of wave packets at different instants. Each of these follows a different trajectory because of the differences in the initial conditions of their motion, preventing a precise control of strong-field-induced electronic dynamics. Intense few-cycle light pulses with adjustable carrier-envelope (C-E) phase hold promise for a marked improvement. With the C-E phase set to make the peak of the oscillating electric field coincide with the pulse peak (blue line in Fig. 1c) and the strength of the field just sufficient to reach the ionization threshold

at the pulse centre, a single, isolated electronic wave packet can be formed. The motion of this wave packet launched into an accurately controlled electric (and magnetic) field at a well-defined instant is determined with the highest possible precision permitted by quantum mechanics. Hence, few-cycle light with controlled electric-field waveforms offers the ultimate control of strong-field-driven atomic, molecular and plasma dynamics. This prospect constitutes the primary motivation for the work reported here.

In the present experiments, we adjust the peak intensity of linearly polarized few-cycle laser pulses such that several electronic wave packets in the vicinity of the pulse peak are set free. First they are removed from their parent ion, but within a laser period they are pulled back by the laser electric field (Fig. 1b). The highest-energy portion of the wave packet re-collides with the ion near the second (counting from the wave packet's 'birth') zero transition of the laser electric field, and results in the emission of an energetic (soft-X-ray) photon[11,13]. Being repeated many times in a multi-cycle laser field, this elementary process results in a series of equidistant emission lines corresponding to high-order odd harmonics of the driver laser light[14] and a sequence of sub-femtosecond bursts in the time domain[15]. By contrast, our few-cycle pulses release only a few wave packets near the pulse centre. The grey arrows in Fig. 1c depict

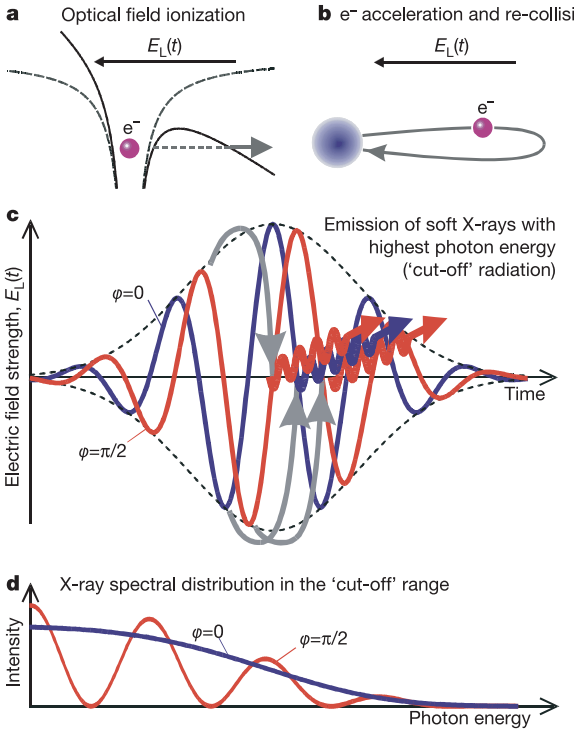

Figure 1 Optical-field ionization and generation of coherent extreme ultraviolet and soft-X-ray radiation from an atom exposed to a strong, linearly polarized, few-cycle light pulse. **a**, The effective Coulomb potential binding valence electrons to the atomic core (dashed curve) is temporarily suppressed around the oscillation peak of the laser electric field. A valence electron can tunnel through or escape above the potential barrier formed by the superposition of the atomic Coulomb field and the instantaneous laser field (solid curve). The electron wave packet that is set free within one-half of the laser period ($T_0 = 2.5$ fs at a wavelength of 750 nm) is temporally confined to less than $T_0/10$ owing to a nonlinear dependence of the ionization probability on the strength of the laser electric field E_L. Atoms exposed to a few-cycle pulse emit one or several wave packets near the pulse peak, depending on the peak intensity (relative to the ionization threshold) and the C-E phase φ. **b**, The freed electron is moved away from the atomic core and then pulled back to it by a linearly polarized field. Re-collision of the electron with its parent ion may trigger several processes, including secondary electron emission, excitation of bound electrons and emission of an energetic (soft-X-ray) photon. **c**, The highest-energy ('cut-off') X-ray photons are emitted near the zero transitions of the laser electric field around the pulse peak. With $\varphi \approx 0$ (cosine waveform, blue line) they are temporally confined to one single burst, whereas $\varphi \approx \pi/2$ (sine waveform, red line) yields two bursts of comparable amplitude separated by $\sim T_0/2$. **d**, As a result, the spectral distribution of the emitted 'cut-off' X-rays is continuous or modulated quasi-periodically, respectively.

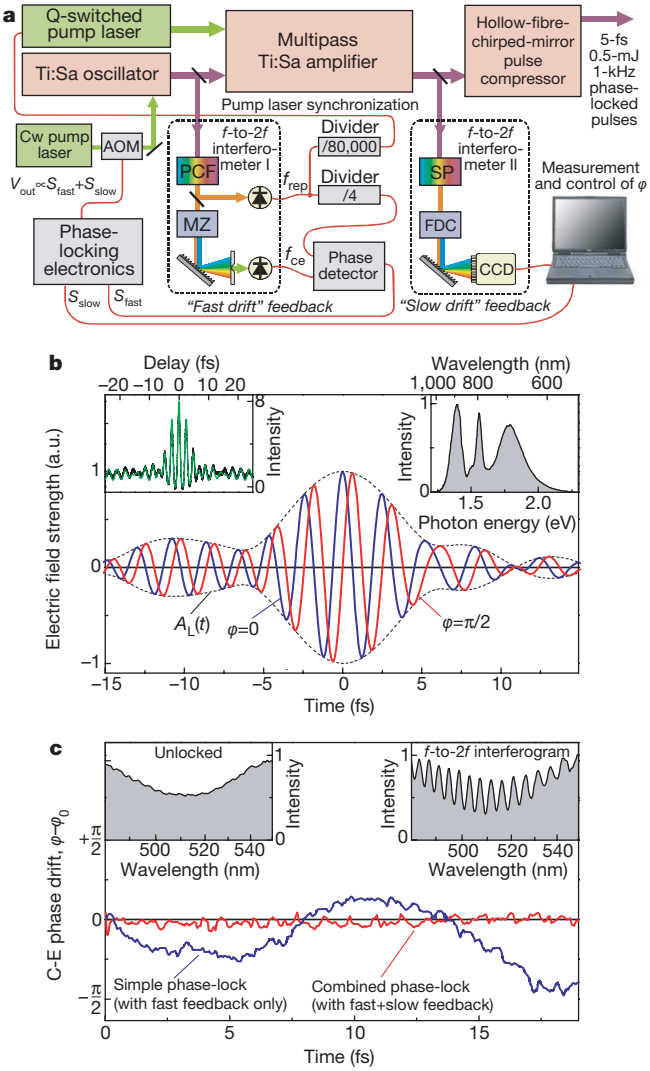

Figure 2 Overview of C-E-phase-stabilized high-power laser system. **a**, Schematic of the laser set-up. AOM, acousto-optical modulator; PCF, photonic crystal fibre; MZ, Mach–Zehnder set-up; SP, 2-mm sapphire plate; FDC, frequency-doubling crystal. The C-E phase of the pulses delivered by the titanium:sapphire (Ti:Sa) oscillator is controlled by tracking the *f*-to-2*f* signal in interferometer I and controlling the pump power (Verdi, Coherent) through a feedback based on the AOM. Frequency dividers /4 and /80,000 are used to derive, respectively, the reference frequency for the stabilization of the phase slip behind interferometer I and the repetition rate of pulses amplified in a multipass amplifier (Femtopower Compact Pro, Femtolasers; pump source: Corona, Coherent). With this technique the C-E phase recurrence of the Ti:Sa oscillator is set such that every fourth pulse (and therefore also every 80,000th pulse) exhibits the same electric-field waveform. The residual drift of the C-E phase behind the laser amplifier is monitored with interferometer II and pre-compensated by shifting accordingly the C-E phase of the oscillator. See Methods for further details. **b**, Pulse properties behind the hollow-fibre-chirped-mirror compressor. The blue and red curves depict possible electric-field waveforms compatible with $A_L(t)$ and $\omega_L(t)$ retrieved from the interferometric autocorrelation (left inset) and the pulse spectrum (right inset) for different settings of the C-E phase; **c**, C-E phase drift versus time with and without slow-drift feedback (compare **a**); insets show the *f*-to-2*f* interference spectrograms recorded with interferometer II. a.u., arbitrary units; f_{rep}, repetition rate of the oscillator; f_{ce}, *f*-to-2*f* beat signal; S_{fast} and S_{slow}, electric signals from the 'fast' and 'slow' feedback loops; V_{out}, amplitude of AOM control voltage.

those that have the highest kinetic energy at re-collision and, consequently, produce the highest-energy (cut-off) X-ray photons. The spectral distribution of these photons depends sensitively on whether they are emitted in a single sub-femtosecond X-ray burst or in a couple of bursts, which can be controlled with the C-E phase of the few-cycle laser pulse (Fig. 1d). Such sub-femtosecond X-ray bursts were recently produced and measured using randomly phased few-cycle light pulses[16,17]. As the emission of two bursts of comparable energy can only occur within a narrow range of C-E phases, statistically, the highest-energy X-ray photons were carried in one dominant burst. Yet, optimization of the excitation conditions for maximum concentration of X-ray emission energy in a single pulse and their accurate reproduction has not been possible with randomly phased laser pulses. Here we report the generation of this radiation—which we do not refer to as high harmonics for the reasons explained below—with phase-stabilized light pulses. The spectral distribution of the highest-energy X-ray photons emerging from the few-cycle-driven ionization process enables us to determine the C-E phase. In combination with standard pulse diagnostics, this approach permits complete characterization of the temporal structure of few-cycle light waveforms (with an ambiguity in the direction of the field).

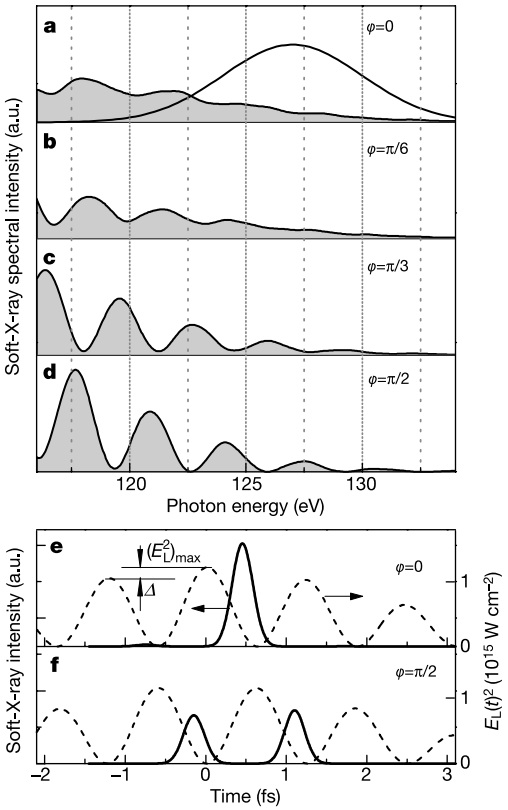

Figure 3 Numerical simulations of few-cycle-driven coherent soft-X-ray emission from ionizing atoms. **a**–**d**, Cut-off-range spectra for different C-E-phase settings of the driving laser pulse. **e**, **f**, The solid curves depict the temporal intensity profile of the cut-off harmonic radiation filtered through a gaussian bandpass filter with a full-width at half-maximum of 7 eV (solid line in **a**), whereas the dashed curves plot $E_L(t)^2$. The parameters of the calculations are as follows: laser pulse duration, $\tau_L = 5$ fs; pulse energy, 0.2 mJ; beam diameter, $2w_L = 122\,\mu$m; medium, neon; pressure, 100 mbar; length, 2 mm. These results, along with previous numerical studies[4,9], fully support our intuitive analysis: the few-cycle cosine wave is predicted to produce a single soft-X-ray burst (filtered in the cut-off, **e**). Deviation of φ from zero gradually suppresses the magnitude of the main burst and gives rise to a satellite spike. The latter becomes most prominent for $|\varphi| \rightarrow \pi/2$ (**f**). In the frequency domain, the isolated pulse emerging for $\varphi = 0$ implies a continuous spectrum (**a**), which gets increasingly modulated with the appearance of the second burst for $|\varphi| \rightarrow \pi/2$ (**b**–**d**). Detailed numerical simulations show that the values of φ corresponding to the smoothest and the most deeply modulated cut-off spectra are shifted by about 20° from the intuitively anticipated values of 0 and $\pi/2$. The relative bandwidth of the cut-off continuum linearly scales with the ratio $\Delta/(E_L^2)_{max}$ (compare **e**), which, in turn, is related to the number of cycles in the optical field, τ_L/T_0. In fact, the continuum bandwidth is as broad as ~20 eV for $\tau_L/T_0 = 2$ and a cut-off photon energy of 125 eV, and shrinks to only 3.8 eV for $\tau_L/T_0 = 5$.

The electric field of a linearly polarized light pulse can be generally written as $E_L(t) = A_L(t)\cos[\omega_L(t)t + \varphi]$. This description includes three physical quantities: the amplitude envelope $A_L(t)$, where t is time, the instantaneous frequency of the field oscillations $\omega_L(t) = \omega_0 + \beta(t)$, where $\beta(t)$ is a possible frequency sweep across the pulse, and the C-E phase φ. In few-cycle pulses, a change in φ affects $E_L(t)$ considerably[2]. Whereas $A_L(t)$ and $\omega_L(t)$ can be obtained from standard pulse diagnostic techniques and flexibly modified in pulse shapers, φ has remained immeasurable so far. In general, pulses delivered by femtosecond lasers have a reproducible envelope and carrier frequency but carry a random C-E phase[2]. It was demonstrated recently that the pulse-to-pulse shift of φ can be tracked in real time and stabilized using a so-called *f*-to-2*f* interferometer[18–21]. In such a scheme, the laser spectrum is broadened to a full octave and the beat between the frequency-doubled low-frequency spectral components and the high-frequency components is detected and used for active phase stabilization.

In our experiments, we amplify phase-stabilized pulses from a sub-10-fs titanium:sapphire (Ti:Sa) laser (seed oscillator) in a multipass chirped-pulse Ti:Sa amplifier operating at a 1-kHz repetition rate (Fig. 2a). Amplification and temporal recompression yield 20-fs, 1-mJ pulses, which are subsequently spectrally broadened by self-phase modulation in a hollow-core waveguide filled with neon gas, and finally compressed on reflection off chirped multilayer mirrors. This system delivers 5-fs, 0.5-mJ pulses with a carrier wavelength of 750 nm (Fig. 2b)[22]. The C-E phase jitter emerging in the waveguide has been measured by comparing the output beam with a reference split off the input beam in a linear interferometer. The jitter is found to be less than 50 mrad (root-mean-square, r.m.s.) owing to the excellent energy stability of the amplified pulses (<1% r.m.s.). The C-E phase can therefore be monitored directly at the output of the amplifier with a broadband *f*-to-2*f* interferometer[23,24].

The drift of the C-E phase can be retrieved from the spectral shift of the recorded pattern of the *f*-to-2*f* spectral interference (right inset in Fig. 2c). In the absence of phase stabilization of the seed oscillator, the *f*-to-2*f* interferogram is completely blurred after approximately 200 laser shots (left inset of Fig. 2b). In contrast, seeding the amplifier with phase-stabilized pulses preserves good fringe visibility over thousands of laser shots. The phase evolution derived from the change of the interference pattern (blue curve in Fig. 2c) appears to be frozen for periods as long as several seconds. Considering the fact that some extra phase noise might be introduced in the measurement process, the blue curve in Fig. 2c accounts for the maximal possible drift of the C-E phase present in the laser system. Due to the slowness of this drift, it can be readily tracked by computer analysis of the *f*-to-2*f* interferogram, and precompensated by a phase offset of opposite sign through a 'slow-drift' feedback loop (Fig. 2a). The simultaneous use of both feedback loops allows stabilizing the C-E phase for extended periods ($\gg$1 minute). The residual variation of the C-E phase retrieved using the in-loop *f*-to-2*f* interferometer is shown by red curve in Fig. 2c. In this case, the upper limit of the C-E phase drift at the output of the laser system can be obtained with an additional, out-of-loop interferometer.

With these intense phase-controlled few-cycle pulses, we can now set out to control electronic motion within the field oscillation cycle of visible light and exploit this technical capability to measure the value of the C-E phase by gauging it with a sensitive strong-field interaction. According to the intuitive insight into the underlying

physics, outlined above, the energetic radiation from an atom ionized by a linearly polarized few-cycle pulse constitutes an excellent candidate for such a C-E-phase calibration. Owing to the fact that the emission of the highest-energy (cut-off) photons is confined to about a single light oscillation period, T_0, the time structure of the generated X-rays is expected to depend sensitively on the C-E phase of the few-cycle driver light. In fact, for a cosine waveform featuring a single strongest half-cycle ($\varphi \approx 0 \pm n\pi$, where $n = 0,1,..$), the highest-energy photons are emitted within a single burst resulting from the wave packet that was 'born' near $t = -T_0/2$ and re-collided with the parent ion in the vicinity of $t = T_0/4$ (Fig. 1c). For a sine waveform ($\varphi \approx \pi/2 \pm n\pi$) there are two most intense half cycles resulting in a pair of most energetic re-colliding wave packets and, correspondingly, two cut-off X-ray bursts emitted near $t = 0$ and $T_0/2$ (Fig. 1c). Therefore, for these two different values of φ we expect distinctly different spectral distributions of the highest energy photons (Fig. 1d): a continuous distribution for $\varphi \approx 0 \pm n\pi$ (where $n = 0,1,..$), and a distribution exhibiting deep (quasi-) periodic modulation in the case of $\varphi \approx \pi/2 \pm n\pi$. These intuitive considerations have been fully confirmed by our numerical simulations[25,26] for the realistic experimental conditions of a macroscopic generation medium. Figure 3 depicts representative results. Our investigations reveal that $\tau_L/T_0 \leq 2.5$ (where τ_L is the pulse width, full-width at half-maximum) is required to produce a soft-X-ray continuum of sizeable relative bandwidth (>10%; that is, >10 eV in the 100-eV range). For pulses that meet this requirement and have a duration close to their bandwidth limit, the above-described dependence of the spectral structure of the cut-off radiation on φ is found to be robust within a broad range of parameters. Consequently, it can be used for calibrating the value of the C-E phase.

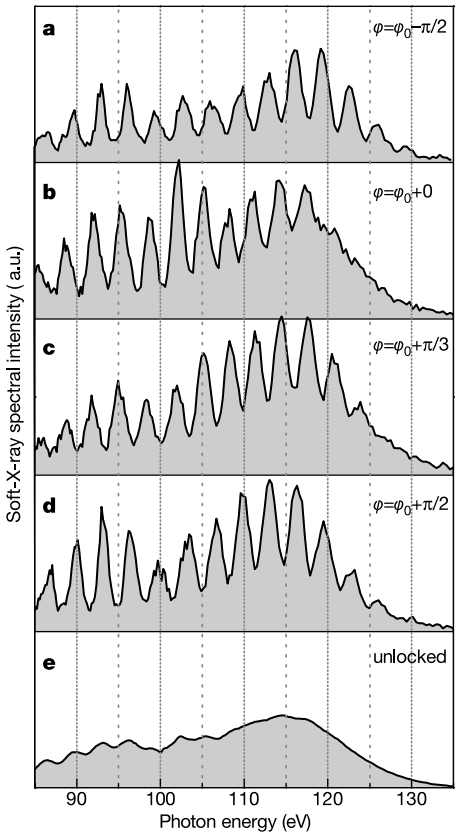

Figure 4 Measured spectral intensity of few-cycle-driven soft-X-ray emission from ionizing atoms. **a**–**d**, Data obtained with phase-stabilized pulses for different C-E-phase settings. **e**, Spectrum measured without phase stabilization. CCD exposure time was 0.5 s in all cases. The coherent energetic radiation was generated by gently focusing 5-fs, 0.2-mJ laser pulses into a 2-mm-long neon gas medium. The on-axis peak intensity of the pump pulse was estimated to be 7×10^{14} W cm^{-2}. The neon gas was supplied in a thin-walled metal tube with a backing pressure of 160 mbar. The pressure in the interaction region, however, was somewhat lower owing to the gas expansion into the surrounding vacuum chamber. Thin zirconium foils were installed in the pathway of the generated soft-X-ray radiation in order to block the laser light as well as low-order harmonics. The high-energy part of the spectrum (above 80 eV) was spectrally analysed with a simple spectrometer consisting of a 10,000 lines mm^{-1} transmission grating and a back-illuminated soft-X-ray CCD camera (Roper Scientific).

We have generated coherent soft X-rays by gently focusing our phase-stabilized 5-fs pulses into a 2-mm-long sample of neon gas. Figure 4 shows a series of soft-X-ray spectra produced under the conditions that are described in Fig. 4 legend for different values of the C-E phase of the 5-fs pump pulses. For a setting of $\varphi = \varphi_0$ (Fig. 4b), a broad structureless continuum appears in the cut-off region ($\hbar\omega > 120$ eV). Notably, with a change of the phase, the continuous spectral distribution of the cut-off radiation gradually transforms into discrete harmonic peaks, with the maximum modulation depth appearing for the settings of $\varphi = \varphi_0 \pm \pi/2$. This behaviour is in agreement with the intuitive picture presented above, and allows us to identify φ_0 as zero with a residual ambiguity of $n\pi$, where n is an integer. This ambiguity in the determination of φ relates to the inversion symmetry of the interaction with the atomic gas medium. In fact, a π-shift in φ results in no change of the light waveform other than reversing the direction of the electromagnetic field vectors. This phase flip does not modify the intensity of the radiated X-ray photons, but it might become observable in photoelectron experiments[8,10].

Another noteworthy feature that has emerged from the soft-X-ray experiments with phase-stabilized pulses is the frequency shift of the harmonic peaks as a function of φ. This effect has been predicted by previous[27] simulations, as well as by our current simulations, and clearly manifests itself in the spectra shown in Fig. 4. This shift is due to a phase shift of the satellite burst with respect to the main X-ray burst, presumably as a consequence of the variation of the field amplitude within T_0 induced by that of the C-E phase. This behaviour reveals that the 'harmonic' fringes visible in the cut-off region of few-cycle-driven high-harmonic spectra do not represent genuine harmonics, because the latter should remain invariant to the change in the C-E phase as long as the laser frequency ω_L is left unchanged. This shift, induced by C-E phase, completely smears the harmonic structure of the near-cut-off soft X-rays generated by our 5-fs pulses in the absence of phase stabilization (Fig. 4e). Real high-order harmonics (invariant to shifts in φ) appear at photon energies some 40% below cut-off (plateau harmonics, not shown in Fig. 4), which are also observed in the absence of phase stabilization. The invariance of these plateau harmonics to shifts in φ confirms the fact that $\omega_L(t)$ is not affected by varying the C-E phase in our experiment.

The periodic spectral modulation present for $\varphi \approx \pi/2$ up to the highest photon energies observed, $\hbar\omega_{cut\text{-}off} \approx 130$ eV (Fig. 4d), completely disappears over a band of ~16 eV in the cut-off range as φ is shifted to zero (Fig. 4b). This is in fair agreement with the 20-eV continuum bandwidth predicted by our simple considerations for a 5-fs, 750-nm ($\tau_L/T_0 = 2$) laser pulse. The C-E phase can be evaluated with the highest possible accuracy by recording pairs of soft-X-ray harmonic spectra at $\varphi_1 = \varphi$ and $\varphi_2 = \varphi + \pi/2$, where φ is varied in small steps. In this method, $\varphi = 0$ (or, equivalently, π) can be identified from a pair of spectra that exhibit, respectively, the smallest and the largest modulation depth in the cut-off range. The current phase and intensity stability of our few-cycle pulses permits identification of a 'cosine' pulse with an accuracy better than $\pi/5$. The obtained value of φ is subsequently used to calibrate the interference pattern recorded in the second f-to-$2f$ interferometer. With this calibration done, we can change φ with an accuracy of better than $\pi/10$ using the interferometer.

In this work we have demonstrated the generation of intense few-cycle light pulses with reproducible temporal evolution of the electromagnetic field. With these controlled intense light waveforms, we have explored the sensitivity of microscopic atomic currents to the timing of light field oscillations with respect to the pulse peak. The spectral distribution of the soft-X-ray radiation emitted by the atomic currents change as this timing is changed by less than 250 as, allowing a calibration of the C-E phase with a precision better than $\pi/5$. Intense few-cycle light pulses with a reproducible and known waveform allow precise control of the emission of an electron wave packet from an atom (or molecule) and its subsequent motion. The emerging field of attosecond physics is expected to benefit from this capability in several ways. First, the re-colliding electron wave packet may serve as a sub-femtosecond excitation pulse for atomic electron dynamics, or as a source of well-controlled, isolated sub-femtosecond X-ray pulses (Fig. 3e). Second, measurement of the shape and chirp[28,29] of sub-femtosecond pulses is becoming feasible by recently demonstrated attosecond diagnostic techniques[16,17]. Third, time-resolved inner-shell spectroscopy[30] could now be extended to tracing atomic processes at an attosecond timescale. Last, extending intense light waveform control to ultrahigh intensities would allow the motion of relativistic electrons to be steered with unprecedented accuracy. □

Methods

C-E phase stabilization loop

The high-power laser set-up (Fig. 2a) incorporates a phase-stabilized 10-fs laser system (FS 800, Menlo Systems). It consists of a dispersive-mirror-controlled Kerr-lens mode-locked Ti:sapphire oscillator (Femtosource Compact Pro, Femtolasers), an *f*-to-2*f* unit ('interferometer I' in Fig. 2a), and phase-locking electronics driving an acousto-optic modulator (AOM in Fig. 2a). About 50% of the output of the oscillator is directed into a 2-cm-long photonic crystal fibre (PCF in Fig. 2a) to broaden the spectrum of the pulses beyond an octave. Subsequently, the low-frequency components f_{low} of the broadened spectrum are frequency-doubled to produce an interference beat with the fundamental light at the high-frequency end of the spectrum, that is, $f_{high} = 2f_{low}$. The optical set-up producing this beat signal is referred to as an *f*-to-2*f* interferometer. The phase of the two interfering quasi-monochromatic wave packets differs by $2\varphi - \varphi + \phi$, where ϕ is an unknown constant phase shift that prevents access to the value of φ in this type of experiment. For practical reasons, ϕ cannot be reliably calibrated from an *f*-to-2*f* set-up. Despite the fact that the value of the C-E phase remains unknown, the information on its drift is sufficient to phase-stabilize the oscillator. In our laser system, the spectrally broadened oscillator pulses are fed into a Mach–Zehnder set-up (MZ in Fig. 2a) that has a frequency-doubling crystal in one of the arms[2,20,21]. The interference with the original spectrum leads to the *f*-to-2*f* beat signal $f_{ce} = \Delta\varphi\, f_{rep}/2\pi$ at around 530 nm, where $\Delta\varphi$ is a pulse-to-pulse shift of the C-E phase. The phase detector compares the electric signal detected at the output of the MZ with a reference, the frequency of which is derived by dividing the repetition rate of the oscillator ($f_{rep} \approx 80$ MHz) by a factor of 4. Forcing the two signals, $1/4\, f_{rep}$ and ω_{CE} to oscillate in phase yields $\Delta\varphi = 1/4 \times 2\pi$ so that every fourth pulse looks alike. The rough adjustment of $\Delta\varphi$ is performed by changing the optical path length through a thin intracavity fused-silica plate. At this stage, φ is approximately reproduced in every fourth round trip in the laser cavity, which results in a quasi-periodic modulation of the *f*-to-2*f* beat signal at $f_{ce} \approx f_{rep}/4 \approx 20$ MHz. Next, to enhance the accuracy of the phase reproducibility, the *f*-to-2*f* beat signal is phase-locked to the $f_{rep}/4$ reference. This phase-locking is achieved by controlling $\Delta\varphi$ via nonlinear effects in the Ti:Sa crystal through variation of the pump intensity[2]. For this purpose, the beam of the continuous-wave (c.w.) pump laser is passed through the AOM, which varies the power of the transmitted beam proportionately to the phase error signal described above. As a result, every fourth pulse, in the 80-MHz pulse train, and therefore also every 80,000th pulse picked by the multipass amplifier, carries the same C-E phase, giving rise to an accurate optical field reproduction in the radiation seeded into the amplifier. To correct additional C-E phase drift emerging during the process of amplification, the spectral interferograms detected behind the amplifier in the second *f*-to-2*f* unit ('interferometer II' in Fig. 2a) are analysed in a personal computer by a Fourier-transform algorithm. The resultant (slowly varying) phase error signal is subsequently combined with the feedback from the phase detector in the first *f*-to-2*f* interferometer and used to control the AOM.

Measurement of phase jitter introduced by the hollow waveguide

The method of (linear) spectral interference was used to assess the C-E phase jitter added by the hollow-fibre chirped-mirror pulse compressor (Fig. 2a). The measurement was performed by splitting off a reference beam behind the multipass amplifier, and interfering it with the spectrally broadened and temporally compressed light. The resultant spectral interferograms, recorded with a CCD (charge coupled device)-based spectrometer, reflected the shot-to-shot phase jitter that has two distinct contributions. The first arises from the mechanical path-length fluctuations of the interferometer arms, and corresponds to a linear variation of the spectral phase. The second represents the shift of the C-E phase resulting from the beam pointing and intensity instabilities of the light coupled into the hollow waveguide. As the C-E phase jitter is frequency-independent, it can be clearly separated from the contribution added by the mechanical arm length drift.

Numerical simulations of the generation and propagation of soft X-rays

We used an improved version of the code first presented in refs 25 and 26. The code solves the wave propagation equations in three dimensions of space, where cylindrical symmetry is assumed for the transverse beam profile, and the slowly evolving wave approximation[9] is used. The atomic dipole response to the laser field was calculated by an extension of the model of Lewenstein *et al.*[14,25], using accurate static field ionization rates obtained from numerical fully quantum-mechanical calculations. Harmonic absorption and diffraction is taken into account, as well as the geometrical (Gouy) phase shift, dispersion introduced by free electrons, ionization energy losses, and the delay due to the refractive index of neutral atoms.

Received 8 November 2002; accepted 3 January 2003; doi:10.1038/nature01414.

1. Steinmeyer, G., Sutter, D., Gallmann, L., Matuschek, N. & Keller, U. Frontiers in ultrashort pulse generation: Pushing the limits in linear and nonlinear optics. *Science* **286,** 1507–1512 (1999).
2. Xu, L., Spielmann, C., Poppe, A., Brabec, T. & Krausz, F. Route to phase control of ultrashort light pulses. *Opt. Lett.* **21,** 2008–2010 (1996).
3. Krausz, F., Brabec, T., Schnürer, M. & Spielmann, C. Extreme nonlinear optics: Exploring matter to a few periods of light. *Opt. Photon. News* **9,** 46–51 (1998).
4. de Bohan, A., Antoine, P., Miloševic, D. B. & Piraux, B. Phase-dependent harmonic emission with ultrashort laser pulses. *Phys. Rev. Lett.* **81,** 1837–1840 (1998).
5. Cormier, E. & Lambropoulos, P. Effect of the initial phase of the field in ionization by ultrashort laser pulses. *Eur. Phys. J. D* **2,** 15–20 (1998).
6. Tempea, G., Geissler, M. & Brabec, T. Phase sensitivity of high-order harmonic generation with few-cycle laser pulses. *J. Opt. Soc. Am. B* **16,** 669–673 (1999).
7. Christov, I. P. Phase-dependent loss due to nonadiabatic ionization by sub-10-fs pulses. *Opt. Lett.* **24,** 1425–1427 (1999).
8. Dietrich, P., Krausz, F. & Corkum, P. B. Determining the absolute carrier phase of a few-cycle laser pulse. *Opt. Lett.* **25,** 16–18 (2000).
9. Brabec, T. & Krausz, F. Intense few-cycle laser fields: Frontiers of nonlinear optics. *Rev. Mod. Phys.* **72,** 545–591 (2000).
10. Paulus, G. G. *et al.* Absolute-phase phenomena in photoionization with few-cycle laser pulses. *Nature* **414,** 182–184 (2001).
11. Corkum, P. B. Plasma perspective on strong-field multiphoton ionization. *Phys. Rev. Lett.* **71,** 1994–1997 (1993).
12. Niikura, H. *et al.* Using correlated pairs for attosecond-resolution molecular wave packet measurements. *Nature* (in the press).
13. Schafer, K. J., Yang, B., DiMauro, L. F. & Kulander, K. C. Above threshold ionization beyond the high harmonic cutoff. *Phys. Rev. Lett.* **70,** 1599–1602 (1993).
14. Lewenstein, M., Balcou, P., Ivanov, M. Y., L'Huillier, A. & Corkum, P. B. Theory of high-harmonic generation by low-frequency laser fields. *Phys. Rev. A* **49,** 2117–2132 (1994).
15. Paul, P. M. *et al.* Observation of a train of attosecond pulses from high harmonic generation. *Science* **292,** 1689–1692 (2001).
16. Hentschel, M. *et al.* Attosecond metrology. *Nature* **414,** 509–513 (2001).
17. Kienberger, R. *et al.* Steering attosecond electron wave packets with light. *Science* **297,** 1144–1148 (2002).
18. Udem, T. *Phasenkohärente optische Frequenzmessungen am Wasserstoffatom* Thesis, Ludwig-Maximilians-Univ. (1997).
19. Telle, H. R. *et al.* Carrier-envelope offset phase control: A novel concept for absolute optical frequency measurement and ultrashort pulse generation. *Appl. Phys. B.* **69,** 327–332 (1999).
20. Jones, D. J. *et al.* Carrier-envelope phase control of femtosecond mode-locked lasers and direct optical frequency synthesis. *Science* **288,** 635–639 (2000).
21. Apolonski, A. *et al.* Controlling the phase evolution of few-cycle light pulses. *Phys. Rev. Lett.* **85,** 740–743 (2000).
22. Sartania, S. *et al.* Generation of 0.1-TW 5-fs optical pulses at a 1-kHz repetition rate. *Opt. Lett.* **22,** 1562–1564 (1997).
23. Kakehata, M. *et al.* Single-shot measurement of carrier-envelope phase changes by spectral interferometry. *Opt. Lett.* **26,** 1436–1438 (2001).
24. Baltuška, A., Fuji, T. & Kobayashi, T. Self-referencing of the carrier-envelope slip in a 6-fs visible parametric amplifier. *Opt. Lett.* **27,** 1241–1243 (2002).
25. Milosevic, N., Scrinzi, A. & Brabec, T. Numerical characterization of high harmonic attosecond pulses. *Phys. Rev. Lett.* **88,** 093905 (2002).
26. Yakovlev, V. S. & Scrinzi, A. High harmonic imaging of few-cycle laser pulses. *Phys. Rev. Lett.* (submitted).
27. Priori, E. *et al.* Nonadiabatic three-dimensional model of high-order harmonic generation in the few-optical-cycle regime. *Phys. Rev. A* **61,** 063801 (2000).
28. Itatani, J. *et al.* Attosecond streak camera. *Phys. Rev. Lett.* **88,** 173903 (2002).
29. Kitzler, M., Milosevic, N., Scrinzi, A., Krausz, F. & Brabec, T. Quantum theory of attosecond XUV pulse measurement by laser dressed photoionization. *Phys. Rev. Lett.* **88,** 173904 (2002).
30. Drescher, M. *et al.* Time-resolved atomic inner-shell spectroscopy. *Nature* **419,** 803–807 (2002).

Acknowledgements We thank H. A. Haus, M. S. Pshenichnikov, G. F. Tempea and R. Kienberger for discussions, and Ch. Warmuth, Z. Cheng and M. Wieland for technical assistance. This work was sponsored by the Fonds zur Förderung der wissenschaftlichen Forschung (Austria) and the European ATTO network. We also thank Femtolasers GmbH and Menlo Systems GmbH for support.

Competing interests statement The authors declare competing financial interests: details accompany the paper on *Nature*'s website (http://www.nature.com/nature).

Correspondence and requests for materials should be addressed to F.K. (e-mail: ferenc.krausz@tuwien.ac.at).

16. Afarinkia, K., Vinader, V., Nelson, T. D. & Posner, G. H. Diels–Alder cycloadditions of 2-pyrones and 2-pyridones. *Tetrahedron* **48,** 9111–9171 (1992).
17. Sauer, J. & Sustmann, R. Mechanic aspects of Diels–Alder reactions: A critical survey. *Angew. Chem. Int. Edn Engl.* **19,** 779–807 (1980).
18. Blake, J. F. & Jorgensen, W. L. Solvent effects on a Diels–Alder reaction from computer simulations. *J. Am. Chem. Soc.* **113,** 7430–7432 (1991).
19. Romesberg, F. E., Spiller, B., Schultz, P. G. & Stevens, R. C. Immunological origins of binding and catalysis in a Diels–Alderase antibody. *Science* **279,** 1929–1933 (1998).
20. Heine, A. *et al.* An antibody exo Diels–Alderase inhibitor complex at 1.95 angstrom resolution. *Science* **179,** 1934–1940 (1998).
21. Chen, J., Deng, Q., Wang, R., Houk, K. & Hilvert, D. Shape complementarity, binding-site dynamics, and transition state stabilization: A theoretical study of Diels–Alder catalysis by antibody 1E9. *Chembiochem* **1,** 255–261 (2000).
22. Hilvert, D., Hill, K. W., Nared, K. D. & Auditor, M-T. Antibody catalysis of a Diels–Alder reaction. *J. Am. Chem. Soc.* **111,** 9261–9262 (1989).
23. Braisted, A. C. & Schultz, P. G. An antibody-catalyzed biomolecular Diels–Alder reaction. *J. Am. Chem. Soc.* **112,** 7430–7431 (1991).
24. Gouverneur, V. E. *et al.* Control of the exo and endo pathways of the Diels–Alder reaction by antibody catalysis. *Science* **262,** 204–208 (1993).
25. Ylikauhaluoma, J. T. *et al.* Anti-metallocene antibodies — a new approach to enantioselective catalysis of the Diels–Alder reaction. *J. Am. Chem. Soc.* **117,** 7041–7047 (1995).
26. Xu, J. *et al.* Evolution of shape complementarity and catalytic efficiency from a primordial antibody template. *Science* **286,** 2345–2348 (1999).
27. Collaborative Computational Project, Number 4. The CCP4 suite: Programs for protein crystallography. *Acta Crystallogr. D* **50,** 760–763 (1994).
28. de La Fortelle, E. & Bricogne, G. Maximum-likelihood heavy-atom parameter refinement for multiple isomorphous replacement and multiwavelength anomalous diffraction methods. *Methods Enzymol.* **276,** 472–494 (1997).
29. Brünger, A. T. *et al.* Crystallography & NMR system: A new software suite for macromolecular structure determination. *Acta Crystallogr. D* **54,** 905–921 (1998).

Supplementary Information accompanies the paper on *Nature*'s website (http://www.nature.com/nature).

Acknowledgements We thank S. Wakatsuki, M. Suzuki and N. Igarashi of the Photon Factory, Japan, for help in data collection at beamline BL18B. This work was supported in part by National Project on Protein Structural and Functional Analyses from the Ministry of Education, Science, Sports and Culture of Japan.

Competing interests statement The authors declare that they have no competing financial interests.

Correspondence and requests for materials should be addressed to H.O. (e-mail: hoik@chem.agr.hokudai.ac.jp) and I.T. (e-mail: tanaka@castor.sci.hokudai.ac.jp).
Structure coordinates have been deposited in the Protein Data Bank under accession code 1IZC.

erratum

Attosecond control of electronic processes by intense light fields

A. Baltuška, Th. Udem, M. Uiberacker, M. Hentschel, E. Goulielmakis, Ch. Gohle, R. Holzwarth, V. S. Yakovlev, A. Scrinzi, T. W. Hänsch & F. Krausz

Nature **421**, 611–615 (2003).

In Fig. 2c of this Letter, the units of time on the *x* axis should be seconds, not femtoseconds. □